Journal of the Korean Physical Society, Vol. 73, No. 9, November 2018, pp. 1393∼1398

High-Performance Compton SPECT Using Both Photoelectric and Compton Scattering Events

Taewoong Lee
RI Applied Research Team, Korea Institute of Radiologic and Medical Sciences, Seoul 01812, Korea

Younghak Kim
Department of Bio-Convergence Engineering, Korea University, Seoul 02841, Korea

Wonho Lee*
School of Health and Environmental Science, Korea University, Seoul 02841, Korea

(Received 2 May 2018, in final form 25 June 2018)

In conventional single-photon emission computed tomography (SPECT), only the photoelectric events in the detectors are used for image reconstruction. However, if the ^{131}I isotope, which emits high-energy radiations (364, 637, and 723 keV), is used in nuclear medicine, both photoelectric and Compton scattering events can be used for image reconstruction. The purpose of our work is to perform simulations for Compton SPECT by using the Geant4 application for tomographic emission (GATE). The performance of Compton SPECT is evaluated and compared with that of conventional SPECT. The Compton SPECT unit has an area of 12 cm $\times$ 12 cm with four gantry heads. Each head is composed of a 2-cm tungsten collimator and a 40×40 array of CdZnTe (CZT) crystals with a 3×3 mm^2 area and a 6-mm thickness. Compton SPECT can use not only the photoelectric effect but also the Compton scattering effect for image reconstruction. The correct sequential order of the interactions used for image reconstruction is determined using the angular resolution measurement (ARM) method and the energies deposited in each detector. In all the results of simulations using spherical volume sources of various diameters, the reconstructed images of Compton SPECT show higher signal-to-noise ratios (SNRs) without degradation of the image resolution when compared to those of conventional SPECT because the effective count for image reconstruction is higher. For a Derenzo-like phantom, the reconstructed images for different modalities are compared by visual inspection and by using their projected histograms in the X-direction of the reconstructed images.

PACS numbers: 87.57.uh
Keywords: Compton SPECT, GATE simulation, CZT crystal, Derenzo-like phantom
DOI: 10.3938/jkps.73.1393

I. INTRODUCTION

High-performance systems that use both photoelectric and Compton scattering events have been developed in tomography. In 2007, Park *et al.* proposed the concept of Compton positron-emission tomography (PET) using Si and a $Bi_4Ge_3O_{12}$ (BGO) detector ring with two different layers [1, 2]. Owing to their high energy and position resolution, CdZnTe (CZT) semiconductor detectors with cross-strip electrodes have been utilized in the development of Compton PET. In 2009, Levin and Pratx developed a prototype Compton PET consisting of CZT detectors and proposed PET imaging using the kinematics of Compton scattering [3, 4]. In 2011, Yoon *et al.* proposed the angular resolution measurement (ARM) method to determine the correct interaction sequence based on the angular difference calculated using the position and energy information for each interaction in Compton PET [5]. However, the conventional single photon emission computed tomography (SPECT) techniques have discarded the Compton scattering events in detectors or used Compton-scattering correction of energy spectra for the reconstruction of the image [6].

Conventional SPECT uses ^{99m}Tc (140 keV), and only the photoelectric events are used for the reconstruction of the image because the photoelectric effect dominates at low energies ($<$ 200 keV). Moreover, the information on the radiation scattered in the detector is not used because the scattering events degrade the quality of the reconstructed image. However, if ^{131}I, which emits several higher energy γ-rays (365, 637 and 723 keV), rather than ^{99m}Tc is used in SPECT, the photoelectric and

*E-mail: wonhol@korea.ac.kr; Fax: +82-2-940-2829

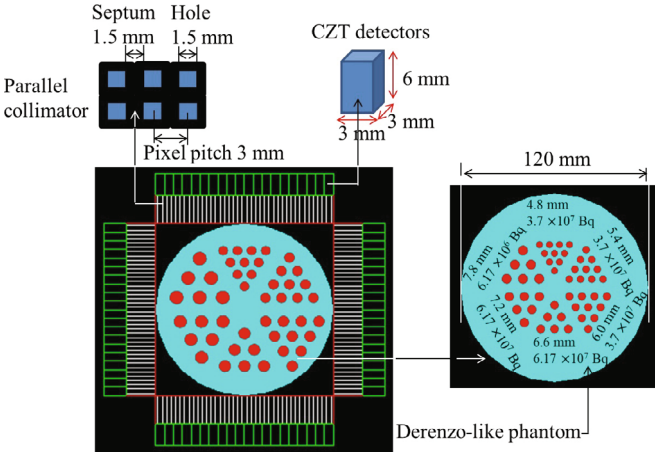

Fig. 1. (Color online) Schematic of the Compton SPECT unit with a Derenzo-like phantom in GATE.

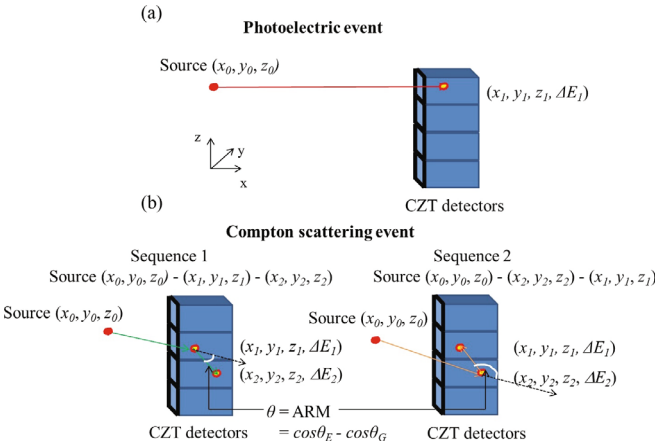

Fig. 2. (Color online) List of events measurable with Compton SPECT: (a) Photoelectric event and (b) Compton scattering event.

the Compton scattering events in the detectors will be comparable [7]. If Compton scattering events are used for effective information in the reconstructed image of SPECT, the detection efficiency and the quality of the reconstructed image can be improved significantly.

In this study, a Compton SPECT technique, which can utilize photoelectric and Compton scattering events for image reconstruction, is designed based on real CZT crystals developed at the Brookhaven National Laboratory (BNL). Moreover, all effective information from the radiations of ^{131}I, whose energies are 364, 637 and 723 keV, was utilized in the reconstructed image. To determine the correct sequential order of the interactions, we applied the angular resolution measurement (ARM) method and the deposited energies of the γ-ray interactions in the detector. Under the correct sequential order, the performance of the Compton SPECT, consisting of a mosaic array of CZT crystals, is evaluated and compared with that of conventional SPECT, which used only photoelectric events.

Table 1. Appropriate energy window for photoelectric and Compton events at various radiation energies.

Energy (keV)	Energy window for photoelectric event (%)	Energy window for Compton event (%)
364	±1.75	±2.47
637	±1.34	±1.90
723	±1.24	±1.75

Table 2. Comparison of the performances estimated for conventional and Compton SPECT.

Diameters of spherical volume sources (mm)	Reconstruction method	FWHM (mm)	NMSE	SNR
12	Conventional SPECT	12.9	0.18	90.3
	Compton SPECT	13.2	0.19	97.7
18	Conventional SPECT	18.4	0.47	52.8
	Compton SPECT	18.9	0.50	64.3
24	Conventional SPECT	24.3	0.33	27.9
	Compton SPECT	24.5	0.39	37.8
30	Conventional SPECT	30.3	0.19	20.1
	Compton SPECT	30.7	0.21	27.9

II. MATERIALS AND METHODS

1. Design parameters for Compton SPECT

To validate the simulation for Compton SPECT, we modeled CZT detectors developed by BNL [8]. A simulation code, the Geant4 application for tomographic emission (GATE 7.0), was used for the Monte Carlo calculations. As shown in Fig. 1, the Compton SPECT unit consisted of four gantry heads composed of a 40×40 mosaic array of CZT detectors of size with a size of $3 \times 3 \times 6$ mm^3. The detector system included parallel-hole collimators to obtain information on the position of the interaction. The hole diameter and the thickness of the parallel-hole collimator were chosen to be 1.5 mm and 30 mm, respectively. The pixel pitch was 3 mm. The acceptable septal thickness was determined to be 1.5 mm, which was the value achievable by a septal penetration of less than 5% at 364 keV [9,10]. The Derenzo-like phantom consisted of a cylinder with a height of 60 mm and containing hot rods of various diameters [11]. The diameters of the various rods positioned in six different segments were 4.8 mm, 5.4 mm, 6.0 mm, 6.6 mm, 7.2 mm, and 7.8 mm, as shown in Fig. 1.

2. Interaction sequence and reconstructed image

As shown in Fig. 2, the Compton SPECT imaging system employed both photoelectric and Compton-

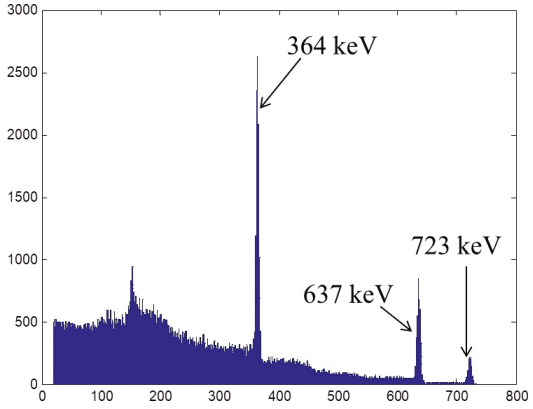

Fig. 3. (Color online) Energy spectrum from Compton SPECT calculated by using GATE.

scattering events for image reconstruction. The Compton scattering events for image reconstruction were based on the Compton-scattering process [12, 13]. The incident photons were scattered in the first detector and subsequently absorbed in the second detector. The two sequences of Compton-scattering events could be estimated as the source-(x_1, y_1, z_1)-(x_2, y_2, z_2) interactions and the source-(x_2, y_2, z_2)-(x_1, y_1, z_1) interactions.

If the location of the source (x_0, y_0, z_0) is known to be at the center of the field of view (FOV), the measured interaction positions and deposited energies can be used to determine the correct sequence by using the ARM method. The cosine values of the scattering angle and the ARM can be determined as follows:

$$\cos\theta_E = 1 - \frac{m_0c^2\Delta E_1}{E_0\Delta E_2}, \tag{1}$$

$$\cos\theta_G = \frac{(x_1-x_0)(x_2-x_1)+(y_1-y_0)(y_2-y_1)+(z_1-z_0)(z_2-z_1)}{\sqrt{(x_1-x_0)^2+(y_1-y_0)^2+(z_1-z_0)^2}\times\sqrt{(x_2-x_1)^2+(y_2-y_1)^2+(z_2-z_1)^2}}, \tag{2}$$

$$\mathrm{ARM} = \theta_E - \theta_G, \tag{3}$$

where m_0c^2 is the rest mass of the electron and $\cos\theta_E$ is the scattering angle calculated based on the energy $(\Delta E_1, \Delta E_2)$ deposited in the detectors. $\cos\theta_G$ is calculated based on the measured interaction position (x_1, y_1, x_2, y_2) and each pixel position on the source plane. A smaller ARM indicates a higher probability for a correct choice of sequence. Hence, the sequence demonstrating a lesser difference between $\cos\theta_E$ and $\cos\theta_G$ should be chosen as the correct sequence.

If the location of the source (x_0, y_0, z_0) is unknown a priori, the correct sequence can be determined by a comparison of the deposited energies at each interaction position. According to Ref. 13, this method, which used a fraction of interactions depositing higher energy, was suggested on the basis of an assumption that the higher count of the correct sequence guaranteed a better reconstruction image [13]. Hence, if the energy of the incident γ-ray is less than 400 keV, less energetic events is selected as the first interaction. On the other hand, if the energy of the incident γ-ray is higher than 400 keV, a higher energy will be deposited in the first interaction. Based on the correct interaction sequence, the first interaction position and the deposited energies can be used for image reconstruction.

In order to reduce the misclassified events among the effective events, we used an energy window for the total energy deposited in the CZT detectors. An energy window that is too narrow will reject not only the misclassified events but also the effective Compton scattering events. In contrast, a broad energy window will allow more effective events and increase the number of misclassified events. Hence, finding a proper energy window for the Compton SPECT is important. The energy window for the effective Compton scattering events can be calculated from the energy resolution of a Compton camera consisting of CZT detectors. The energy resolution (ΔE) of the Compton camera is defined by [14]

$$E = \sqrt{(\Delta E_{\text{First CZT detector}})^2 + (\Delta E_{\text{second CZT detector}})^2}. \tag{4}$$

Table 1 shows the appropriate energy window of the total energy sum for photoelectric and Compton events at various energies.

The images obtained using proper energy windows were reconstructed using 2D filtered back projections (FBP) with a Hann filter. A 3.40-GHz CPU in a personal computer (i7-6700) and MATLAB2010 were used to reconstruct the source image. In order to compare and evaluate the qualities of the reconstructed images obtained from conventional SPECT and Compton SPECT, we used three types of methods. First, the signal-to-noise ratio (SNR) and the full width at half maximum (FWHM) of the reconstructed images were calculated using spherical volume sources of various diameters. The SNR can be calculated using the following equation:

$$\mathrm{SNR} = \frac{\bar{s}}{\sqrt{\frac{\sum(x_i-\bar{x})^2}{n}}}, \tag{5}$$

Table 3. Comparison of the effective counts for each modality.

Events used for image reconstruction	Effective counts for each energy			
	364 keV	637 keV	723 keV	364 keV + 637 keV + 723 keV
Conventional SPECT (Only photoelectric)	1.16×10^6	4.77×10^5	1.71×10^5	1.75×10^6
Compton SPECT (photoelectric + Compton)	1.97×10^6	8.95×10^5	2.58×10^5	3.12×10^6

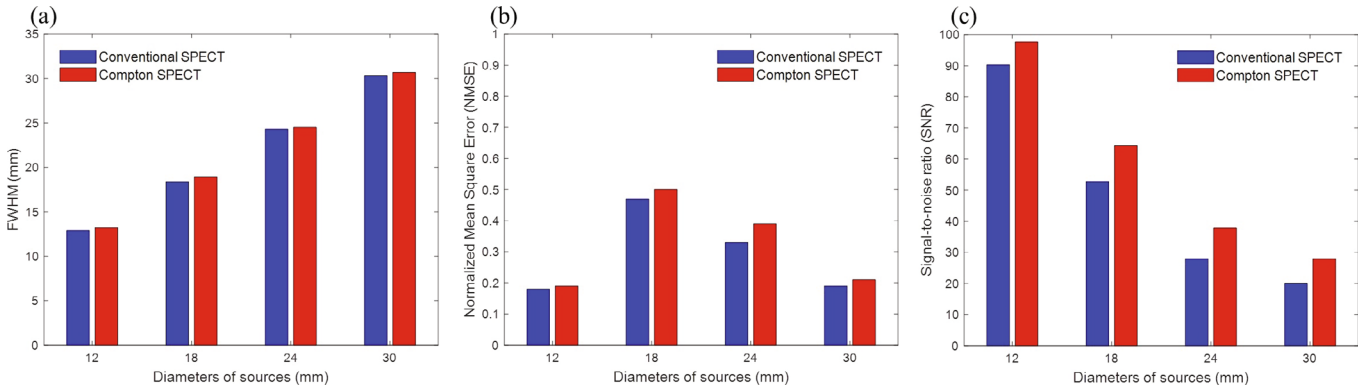

Fig. 4. (Color online) (a) FWHMs, (b) NMSEs, and (c) SNRs of images reconstructed using conventional SPECT and Compton SPECT with a Hann filter.

where $\bar{s}$ is the average value of the source pixels including the maximum pixel, x_i and $\bar{x}$ are the value of each pixel excluding the source pixels and the average of x_i, respectively, and n is the number of pixels x_i. Second, the values of normalized mean square error (NMSE) were compared for each modality. The NMSE can be calculated using the following equation [15]:

$$\text{NMSE} = \frac{\sum_{i=1}^{M}\sum_{j=1}^{N}(I_{\text{f}}(i,j) - I_{\text{T}}(i,j))^2}{\sum_{i=1}^{M}\sum_{j=1}^{N}(I_{\text{n}}(i,j) - I_{\text{T}}(i,j))^2}, \qquad (6)$$

where I_{f} and I_{n} are the filtered and the original images (simple back-projection), respectively, and I_{T} is the true image (noise free). Finally, the reconstructed images obtained using the Derenzo-like phantom were compared for each modality by using visual inspection, spatial resolution, and effective counts.

The most significant ^{131}I γ-ray emissions are at 364 keV (82%), 637 (7.2%), and 723 keV (1.8%) [16]. Hence, the energies of various γ-rays emitted from the ^{131}I radiation source are used in the GATE simulation. Therefore, the simulated energy spectrum from Compton SPECT includes γ-rays whose main energy peaks were 364 keV, 637 keV, and 723 keV as shown in Fig. 3. The total number of γ-rays emitted from the source was 37 million photons.

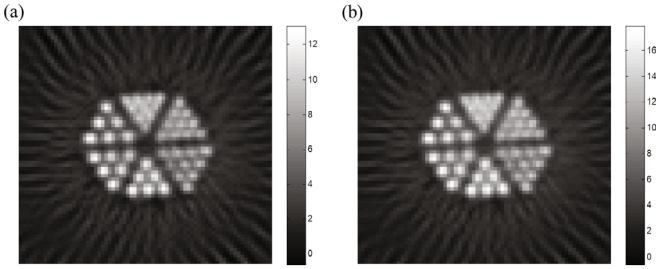

Fig. 5. Reconstructed images of a Derenzo-like phantom for visual inspection: (a) conventional SPECT and (b) Compton SPECT.

III. RESULTS

After a proper energy window had been chosen, the spherical volume sources of various diameters were reconstructed by using FBPs with a Hann filter, and the FWHMs and the SNRs of the reconstructed image were measured for each modality. All effective information from the different energies of ^{131}I, including of 364, 637 and 723 keV, was utilized in the reconstructed image. The FWHMs of the simulation results were generally consistent with the diameters of the spherical volume sources. Because the effective counts in Compton SPECT is increased, the SNRs of Compton SPECT were high when compared to those of conventional SPECT whereas the FWHMs and the NMSEs of both modalities were similar. As shown in Fig. 4 and Table 2, the re-

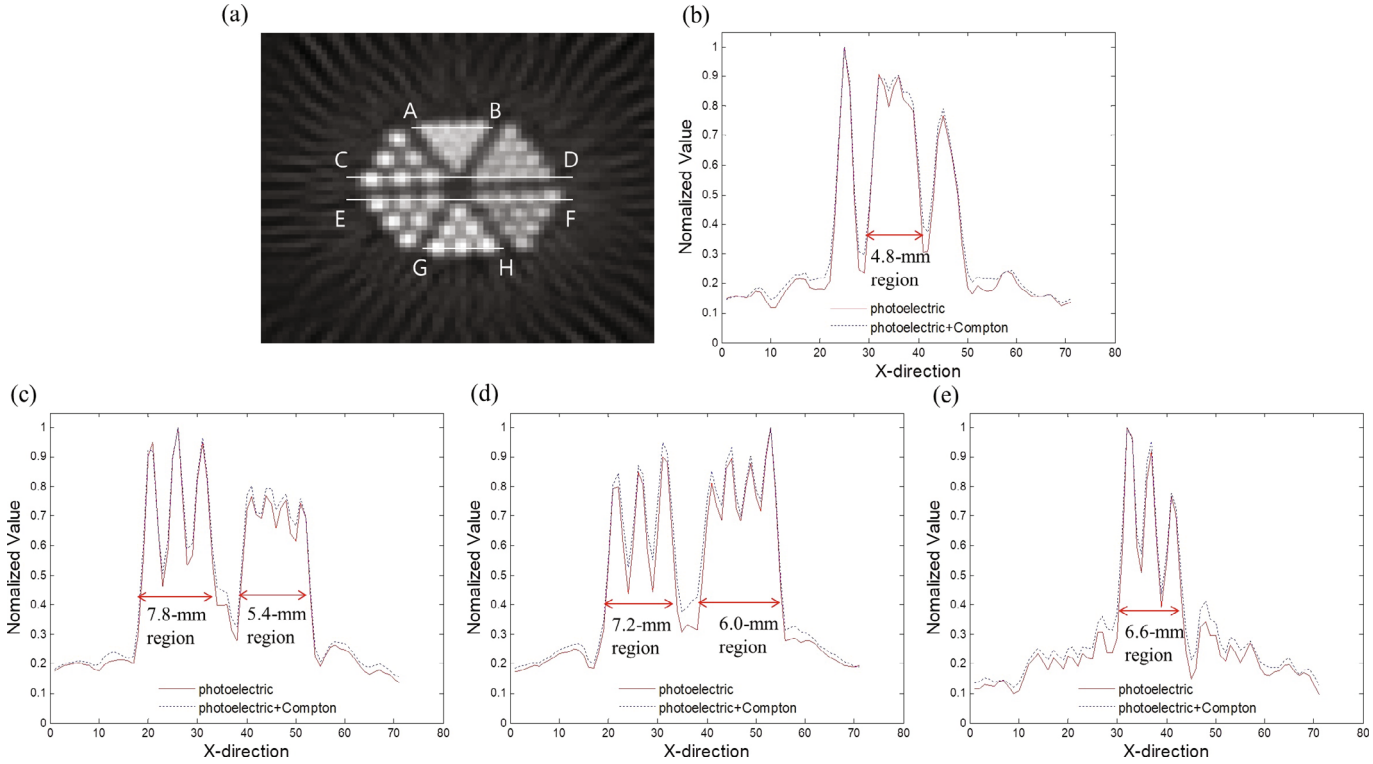

Fig. 6. (Color online) Cross section of each modality from the reconstructed image: (a) reference image, (b) A to B, (b) C to D, (b) E to F, and (b) G to H.

sults prove that the performance of Compton SPECT is better than that of conventional SPECT.

To evaluate the visual inspection and spatial resolution, we utilized the Derenzo-like phantom. The cross-sectional views of the phantom were reconstructed using FBP with a Hann filter. Figures 5 and 6 show the reconstructed images and their projected histograms in the X-direction, respectively. When the diameters of the rods in conventional SPECT and Compton SPECT were greater than 5.4 mm, the rods were completely distinguishable, as shown in Fig. 6. With the energy of the incident radiation was increased, the probability of Compton scattering events increased. Hence, in all simulations, the total number of effective events for the Compton SPECT was higher than that obtained using conventional SPECT as shown in Fig. 7 and Table 3.

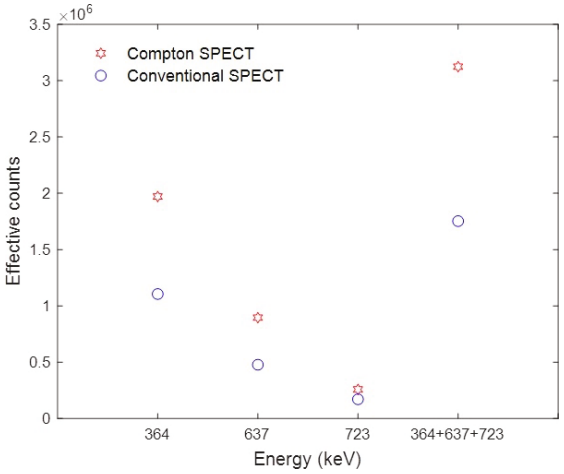

Fig. 7. (Color online) Effective counts for each modality from the reconstructed image.

IV. CONCLUSION

The performance of Compton SPECT using both photoelectric and Compton scattering events was evaluated and compared with that of conventional SPECT, which used only photoelectric events. The proper energy window for both photoelectric and Compton scattering events and the correct interaction sequence were applied for Compton SPECT. The effective events of Compton SPECT were higher than those obtained using conventional SPECT. The reconstructed images obtained using spherical volume sources of various diameters and Derenzo-like phantoms demonstrated that the performance of Compton SPECT was improved without degrading the image resolution. In conclusion, the quantitative evaluation based on the SNR and the effective counts proved the superiority of Compton SPECT over conventional SPECT.

ACKNOWLEDGMENTS

This work was supported by the Nuclear Safety Research Program through the Korea Foundation of Nuclear Safety (KoFONS) using the financial resource granted by the Nuclear Safety and Security Commission (NSSC) of the Republic of Korea (No. 1603015). This work was also supported by a Korea University grant (K1808611).

REFERENCES

[1] S-J. Park, W. L. Rogers, S. Huh, H. Kagan, K. Honscheid, D. Burdette, E. Chesi, C. Lacasta, G. Llosa, M. Mikuz, A. Studen, P. Weilhammer and N. H. Clinthorne, Phys. Med. Biol. **52**, 2807 (2007).
[2] S-J. Park, W. L. Rogers and N. H. Clinthorne, IEEE Trans. Nucl. Sci. **54**, 1589 (2007).
[3] C. S. Levin, M. P. Tornai, S. R. Cherry, L. R. MacDonald and E. J. Hoffman, IEEE Trans. Nucl. Sci. **44**, 218 (1997).
[4] G. Pratx and C. S. Levin, Phys. Med. Biol. **54**, 5073 (2009).
[5] C. Yoon, W. Lee and T. Lee, Nucl. Instrum. Meth. A **652**, 713 (2011).
[6] K. F. Koral, X. Wang, W. L. Rogers, N. H. Clinthorne and X. Wang, J. Nucl. Med. **29**, 195 (1988).
[7] G. F. Knoll, *Radiation Detection and Measurement* (Wiley, New York, 2010), 4th edition, Chap. 2, p. 48.
[8] A. E. Bolotnikov, G. S. Camarda, G. A. Carini, G. W. Wright, D. S. McGregor, W. McNeil and R. B. James, Proc. SPIE **5540**, 33 (2004).
[9] A. E. Bolotnikov, G. S. Camarda, G. Carini, Y. Cui, K. T. Kohman, L. Li, M. B. Salomon and R. B. James, Proc. IEEE Trans. Nucl. Sci. **R05-2**, 3622 (2006).
[10] M. J. Macey, E. J. Grant, J. E. Bayouth, H. B. Giap, S. J. Danna, R. Sirisriro and D. A. Podoloff, Med. Phys. **22**, 1637 (1995).
[11] C. Beijst, M. Elschot, M. A. Viergever and H. Jong, J. Nucl. Med. **56**, 476 (2015).
[12] F. Boisson, D. Zahra, A. Parmar, M-C Gregoire, S. R Meikle, H. Hamse and A. Reilhac, J. Nucl. Med. **54**, 1833 (2013).
[13] Y. F. Du, Z. He, G. F. Knoll, D. K. Wehe and W. Li, Nucl. Instrum. Meth. A **457**, 203 (2001).
[14] S. Watanabe, T. Tanaka, K. Nakazawa, T. Mitani, K. Oonuki, T. Takahashi, T. Takashima, H. Tajima, Y. Fukazawa, M. Nomachi, S. Kubo, M. Onishi and Y. Kuroda, IEEE Trans. Nucl. Sci. **52**, 2045 (2005).
[15] E. Michel-González, M. H. Cho and S. Y. Lee, BioMed. Eng. Online **10**, 1 (2011).
[16] R. Barquero, H. P. Garcia, M. G. Incio, P. Minquez, A. Cardenas, D. Martínez and M. Lassmann, Phys. Med. Biol. **62**, 909 (2017).